

1 **Spurious rollover of wave attenuation rates in sea ice**
2 **caused by noise in field measurements**

3 **Jim Thomson^{1,5}, Lucia Hošeková^{1,2}, Michael H. Meylan³, Alison L Kohout⁴,**
4 **Nirnimesh Kumar⁵**

5 ¹Applied Physics Laboratory, University of Washington

6 ²Department of Meteorology, University of Reading

7 ³School of Mathematical and Physical Sciences, The University of Newcastle, Callaghan, NSW 2308,
8 Australia.

9 ⁴National Institute of Water and Atmospheric Research, Christchurch, New Zealand

10 ⁵Department of Civil and Environmental Engineering, University of Washington

11 **Key Points:**

- 12 • Noise in raw wave data adds spurious energy to observed wave spectra.
13 • The noise energy causes a bias in the attenuation rates inferred from observed wave
14 spectra.
15 • The bias is a strong function of frequency and explains the rollover in attenuation
16 rates reported in several previous studies.

Corresponding author: Jim Thomson, jthomson@apl.washington.edu

Abstract

The effects of instrument noise on estimating the spectral attenuation rates of ocean waves in sea ice are explored using synthetic observations in which the true attenuation rates are known explicitly. The spectral shape of the energy added by noise, relative to the spectral shape of the true wave energy, is the critical aspect of the investigation. A negative bias in attenuation that grows in frequency is found across a range of realistic parameters. This negative bias decreases the observed attenuation rates at high frequencies, such that it can explain the rollover effect commonly reported in field studies of wave attenuation in sea ice. The published results from four field experiments are evaluated in terms of the noise bias, and a spurious rollover (or flattening) of attenuation is found in all cases. Remarkably, the wave heights are unaffected by the noise bias, because the noise bias occurs at frequencies that contain only a small fraction of the total energy.

Plain Language Summary

Many previous studies have determined the rate at which ocean surface waves decay as they travel through sea ice. This work identifies a systematic bias in those results, using both published data and synthetic data to demonstrate the effect. The bias reconciles an existing debate on the physical mechanisms causing waves to decay in sea ice.

1 Introduction

Ocean surface wave attenuation in sea ice is an established phenomenon (Squire, 2007, 2020) and has been extensively studied using field measurements of wave energy E as a function of frequency f . The attenuation of spectral wave energy $E(f)$ is often expressed as an exponential decay with distance x , such that

$$E(f, x) = E(f, 0)e^{-\alpha(f)x}. \quad (1)$$

The attenuation rate α controls the reduction of wave energy from the incident waves in open water ($x = 0$) to some position within the sea ice. The attenuation rate is then a function of frequency, most commonly a power law,

$$\alpha(f) = af^b, \quad (2)$$

where a and b are constants determined for different ice types during previous studies. Meylan et al. (2018) provide a comprehensive review of the frequency dependence of $\alpha(f)$.

Although $\alpha(f)$ is generally thought to increase with frequency f , many field experiments have suggested a “rollover” in which $\alpha(f)$ eventually decreases at the highest frequencies. These are frequencies commonly referred to as the “tail” of the wave energy spectrum. Wadhams (1975) first noted the rollover, and it was described more fully in the seminal work of Wadhams et al. (1988), who find a rollover in the spectral attenuation rates across many experiments with varying ice types and wave conditions. The rollover is challenging to diagnose because most field observations simply provide the ratio of energy at different locations $E(f, x_1), E(f, x_2)$ and not the actual loss of energy caused by the sea ice. Wadhams et al. (1988) describes two possible mechanisms that might cause the observed rollover, both of which essentially replace (or input) some of the wave energy at high frequencies: 1) input of addition wave energy by wind, and 2) nonlinear transfer of wave energy from lower frequencies to higher frequencies. Masson and LeBlond (1989) consider this further and suggest that winds can input considerable energy into waves in partial ice cover. The various field experiments in Wadhams et al. (1988) dataset report the rollover effect in a range of conditions, including very light winds and small waves with little likelihood of significant nonlinearity. The ubiquity of the rollover is difficult to explain by the two above mechanisms alone.

Recent work has explored both mechanisms suggested by (Wadhams et al., 1988), including a more thorough framework for nonlinear transfers (Polnikov & Lavrenov, 2007) and testing wind input effects (Li et al., 2017; Rogers et al., 2016). Particularly, Li et al. (2017) provide a comprehensive treatment of wind input using modern field observations and a spectral wave model. They conclude that wind input at high frequencies is sufficient to replace some of the wave energy attenuated at high-frequencies, such that reanalysis of the data no longer indicates a rollover in the spectral attenuation rates (though a rollover does appear without considering wind input).

Here, we explore instrument noise as another possible explanation for the emergence of spurious rollovers in attenuation rates from field experiments. Assuming that the noise in the raw data are random errors with Gaussian statistics, the noise will contribute additional variance to the raw data, and this will elevate the spectral wave energy densities $E(f, x)$ determined from the raw data. In terms of variance, this bias in energy will always be positive, even though the actual errors are symmetric with zero-mean. According to the Bienayme theorem, the total variance (energy) will be the sum of the true variance from the wave signal and the variance from the noise, because there are no cross-terms from these uncorrelated signals. Following Parseval’s theorem, this variance is preserved in the calculation of frequency spectra, such that

$$E(f, x) = E_s(f, x) + E_n(f). \quad (3)$$

The observed wave energy spectra $E(f, x)$ is thus a sum of the energy in the wave signal $E_s(f, x)$ and the variance added by instrument noise $E_n(f)$. Although the assumption of Gaussian errors in the raw data would result in a constant “white” spectral shape for $E_n(f)$, the effects of filters and other processing may produce an $E_n(f)$ that is a strong function of frequency. This will be explored in the Methods section.

Previous studies have been well-aware of instrument noise and typically applied cut-off levels below which $E(f, x)$ observations are not used. However, the spectral shape of the noise energy $E_n(f)$ has not been considered, nor have the possible effects of instrument noise on the shape of the spectral attenuation. Most importantly, the value of $E_n(f)$ will remain at the same level while $E_s(f, x)$ decreases with x due to attenuation by sea ice, such that the relative amount of noise increases with distance. For example, Cheng et al. (2017) tried to avoid noise contamination by using a constant cutoff of $E(f, x) > 10^{-5} \text{ m}^2/\text{Hz}$ in processing data from the Arctic Sea State experiment (Thomson et al., 2018). This choice of noise floor is coincidentally the same as the cutoff in (Wadhams et al., 1988). Even though Cheng et al. (2017) did not observe a rollover, they did find a flattening of attenuation rate α at high frequencies and large distances, which they attributed to wind input. More critically, Meylan et al. (2014) did not see a rollover in attenuation rates when analyzing Antarctic wave data with a constant cutoff level of $E(f, x) > 10^{-2}$, yet Li et al. (2017) analyzed the same data with a much lower cutoff and did see a strong rollover in attenuation rate.

Here, we present a framework to understand the bias in attenuation caused by the spectral slope of energy from noise $E_n(f)$ relative to the spectral slope of energy from the wave signal $E_s(f)$. We revisit four different field experiments from the literature to confirm assumptions about the shape of $E_n(f)$ with empirical evidence in the observed energy spectra. We then create synthetic wave energy spectra with known spectral attenuation rates, and then explore the inferred attenuation rates after the variance from instrument noise is added to the synthetic spectra. The general parametric form of bias in attenuation is also derived. The discussion focuses on the spurious nature of previous ‘rollover’ results and presents recommendations for avoiding noise bias in using field observations of wave spectra in ice.

Table 1. Case studies and input parameters for spectral noise effects. The incident wave energies and true attenuation rates are reported for the peak frequency f_p .

Case	$E(f_p, 0)$ [m ² /Hz]	$\alpha_t(f_p)$ [1/m]	b	H_n [m]	r	x [m]
CODA 2019	2e0	1e-4	2	0.10	-4	0-6e3
SeaState 2015	1e1	1e-5	2	0.03	-4	0-100e3
SIPEX 2012	1e1	1e-5	2	0.03	-4	0-250e3
STiMPI 2000	1e0	5e-5	3	0.15	-4	0-100e3

2 Methods

2.1 Specification of case studies

Case studies are chosen to span a wide range of methodologies and published spectral attenuation rates. Not all of these cases reported a complete rollover in published attenuation rates; the intent is to show the full range of noise effects on attenuation estimates. The true attenuation rate $\alpha_t(f) = af^b$ specified for each case study is selected to match the attenuation determined at the peak frequency f_p , since that is most likely to be robust to noise effects preferentially affecting the higher frequencies. Table 1 summarizes the conditions for each case study and the parameters used to create synthetic (true) spectra with added noise. Case studies are referred to by experiment name, rather than the publication(s) of those results.

The first two case studies use observations from SWIFT buoys (Thomson, 2012), which use GPS velocities in onboard processing (Herbers et al., 2012) and accelerometer data in post-processing. The first case was collected in 2019 along the coast of Alaska in pancake ice as part of the Coastal Ocean Dynamics in the Arctic (CODA) program. The second case was collected in 2015 in the Beaufort Sea in pancake ice (Wave Experiment 3) as part of the Arctic Sea State program (Rogers et al., 2016; Cheng et al., 2017; Thomson et al., 2018). The third case uses observations from custom buoys during SIPEX in the Antarctic Marginal Ice Zone (MIZ) in 2012, as described in Kohout et al. (2014, 2015). The fourth case uses observations from custom buoys during STiMPI in the Weddell Sea in pancake ice in 2000, as described in Doble et al. (2015).

2.2 Spectral energy of the wave signal, $E_s(f)$

Ocean waves typically have an energy spectrum with a power law in the spectral tail (i.e., frequencies above the peak frequency f_p) and the overall level can be described by the conventional definition of the significant wave height H_s ,

$$E_s(f > f_p, x) \sim f^q \quad H_s = 4\sqrt{\int E_s(f)df}. \quad (4)$$

In open water, we expect the familiar shape $q = -4$ of the equilibrium tail (Phillips, 1985; Thomson et al., 2013; Lenain & Melville, 2017). Figure 1 shows the energy spectra from observations in the four case studies, which are bin-averaged by H_s and presented in logarithmic space to visualize the f^q dependence. The $q = -4$ shape is clear for open water observations (which are the largest H_s bins) in the CODA 2019 and SeaState 2015 case studies. This $q = -4$ shape in the spectrum is related to a wave field with constant geometric steepness of the waves themselves, expressed as a spectrum of mean-square-slope $mss(f) = E_s(f)f^4$ that has a constant level in f (see (Thomson et al., 2013)).

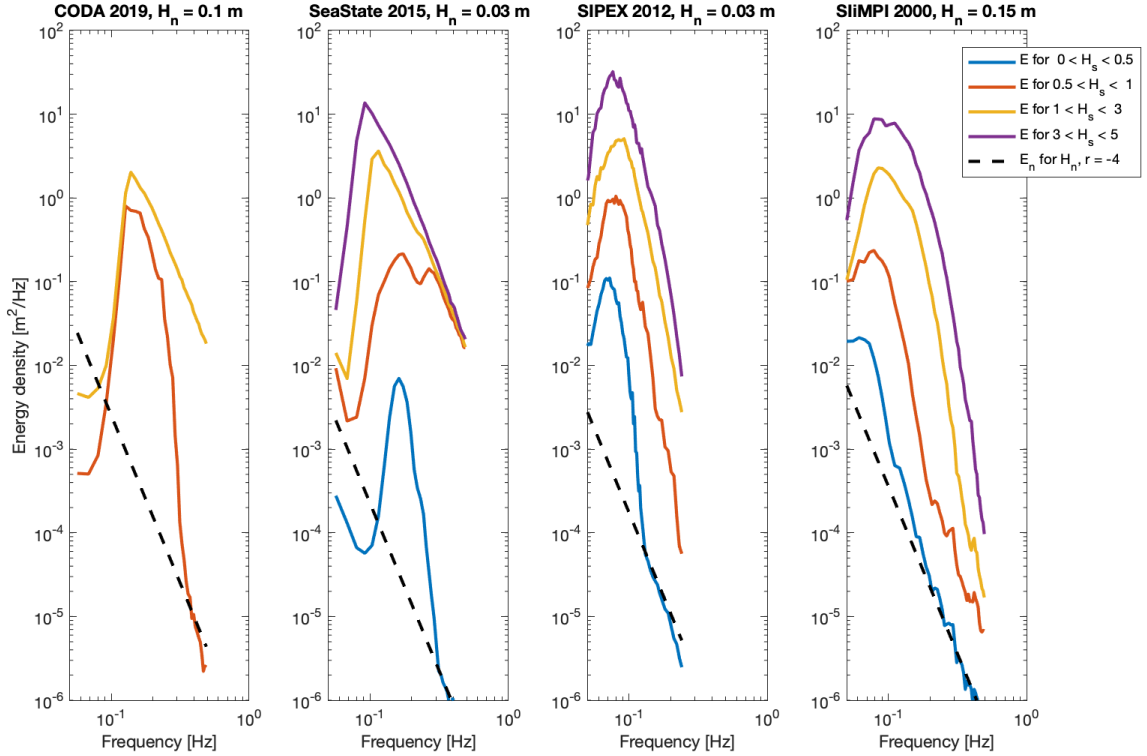


Figure 1. Wave spectra from actual field observations (not synthetic) during each of the four case studies. Spectra are binned by wave height (see legend), and a dashed black line shows the estimated noise energy following Eq. 5.

142 In sea ice, the spectral shape is typically observed to be much steeper ($q < -4$),
 143 which is consistent with largest H_s bins in the SIPEX 2012 and STiMPI 2000 case stud-
 144 ies (Figure 1). These experiments did not include wave observations in open water, so
 145 all wave spectra already have slopes $q < -4$. This high-frequency tail and the implied
 146 changes for wave steepness are the focus of the present study.

147 2.3 Spectral energy of noise, $E_n(f)$

148 There is additional variance (energy) from noise $E_n(f)$ in observed wave spectra,
 149 following Eq. 3. The energy from noise has a generic frequency exponent r and is scaled
 150 with a noise height H_n (analogous to significant wave height):

$$E_n(f) \sim f^r, \quad H_n = 4\sqrt{\int E_n(f)df}. \quad (5)$$

151 The noise height H_n is thus four times the standard deviation of the Gaussian random
 152 noise in the raw measurements of wave elevations. Note, again, that the effect of noise
 153 in the raw data is to increase the total variance, such that the noise height H_n is a bias
 154 in the true wave height H_s , not a symmetric error.

155 The noise height H_n is used as a general characterization of the level of noise $E_n(f)$,
 156 though wave elevations rarely are measured directly. The type of sensor used for the raw
 157 measurements and the subsequent processing to estimate wave elevations will control the

158 frequency exponent r . The expected exponents are $r = -4$ for the double-integration
 159 of accelerometers, or $r = -2$ for the single-integration of GPS velocities, or $r = 0$ (white
 160 noise) from direct measurements of heave (such as from an altimeter or LIDAR).

161 Figure 1 shows the spectral shape of energy from noise for each case study, with
 162 H_n values determined from sensor specifications. These shapes are the result of accelerom-
 163 eter noise that is purely random (white) noise and becomes $r = -4$ with double inte-
 164 gration in time. Each integration in time is equivalent to a factor f^{-1} , and then the f^{-2}
 165 effect from double integration is squared to get f^{-4} when calculating energy (instead of
 166 amplitude). For each experiment, the wave spectra in Figure 1 show the clear effects of
 167 the noise energy as a change in the slope of the spectra at the higher frequencies of the
 168 smallest H_s bin. Although all of the experiments in Figure 1 use accelerometer measure-
 169 ments with an effective $r = -4$ shape in noise energy, it is important to note that other
 170 experiments may have different measurements. One such example is Arduin et al. (2020),
 171 who use GPS velocities as the raw data and thus likely have noise energy with an $r =$
 172 -2 shape.

173 The dashed black lines in Figure 1 show the noise energy $E_n(f)$ for each case study.
 174 For CODA 2019 and SeaState 2015, these are determined empirically by collecting raw
 175 data on land with a stationary SWIFT buoy. For SIPEX 2012 and STiMPI 2000, these
 176 are inferred from the change in slope in the tail of the spectrum during small H_s con-
 177 ditions. The observed change in the slope of $E(f)$ would imply that the geometric wave
 178 steepness of the waves at the highest frequencies is much steeper than at other frequen-
 179 cies. There are no visual observations to support such an abrupt change in the waves,
 180 and instead, we interpret this change in the slope of $E(f)$ as the emergence of noise from
 181 the double-integration of the raw accelerometer data. In summary, when H_s is small, $E_n(f) >$
 182 $E_s(f)$ at the higher frequencies, even though $H_n < H_s$.

183 The additional energy from the instrument noise $E_n(f)$ makes it impossible to mea-
 184 sure energy less than the dashed lines, so when the wave signal $E_s(f)$ becomes weak, the
 185 observed spectra $E(f)$ converge to the dashed lines of $E_n(f)$. When waves are larger,
 186 the noise energy is a negligible fraction of the total energy, and the effects are not read-
 187 ily detected in the spectral shape. Although both CODA 2019 and SeaState 2015 use
 188 SWIFT buoys, the effective H_n is different between these experiments because of differ-
 189 ent filters used to suppress low-frequency drift during the double integration of accelerom-
 190 eter data. Although both the SeaState 2015 and SIPEX 2012 datasets have $H_n = 3$
 191 cm, the spectral levels of $E_n(f)$ are slightly different because the processed spectra have
 192 different resolution in frequency df (see Eq. 5).

193 2.4 Synthetic spectra

194 In the synthetic tests that follow, the incident open-water wave spectra $E_s(f, x =$
 195 $0)$ are specified using Pierson–Moskowitz spectra for fully developed seas, following Alves
 196 et al. (2003). In open water, this $q = -4$ (Eq. 4) shape is known to persist even in the
 197 case of a pure swell without wind (Vincent et al., 2019), though the Pierson–Moskowitz
 198 spectra was developed for a pure wind sea. The synthetic wave spectra use a frequency
 199 range of $0.05 < f < 0.5$ Hz and a resolution $df = 0.01$ Hz, which is similar to many
 200 modern wave buoys.

201 A given incident wave spectrum $E(f, 0) = E_s(f, 0) + E_n(f)$, designed to match
 202 a given case study, is attenuated with distance x into the ice at regular intervals simi-
 203 lar to the measurements from that case study. This noise is not cumulative in x and is
 204 assumed independent of the wave signal; it is a specified additional spurious energy for
 205 each observation $E(f, x)$. Using a specified (true) attenuation rate $\alpha_t(f)$ with a frequency
 206 exponent b (Eq. 1), a true wave spectrum $E_s(f, x)$ at each distance is obtained. This true
 207 spectrum already includes the energy from noise $E_n(f)$ added in the incident wave spec-
 208 trum at $x = 0$ (Eq. 4), but it does not include the energy from noise of the other mea-

209 surement at position x . That noise energy is explicitly added to create total spectra, $E(f, x)$,
 210 following Eq. 3. The key point is that the energy of the noise does not decay with dis-
 211 tance x , though the wave energy does, and each total spectrum has noise energy added
 212 independently. The noise energy added to the incident wave spectrum $E(f, 0)$ likely has
 213 negligible effects, because the wave energy is generally much larger than the noise en-
 214 ergy in defining $E(f, 0)$ at the ice edge. Farther into the ice, however, the noise energy
 215 in any particular measurement may be a much more significant fraction of the observed
 216 energy $E(f, x)$, especially for the higher frequencies.

217 **2.5 Inferred attenuation rates from spectra with noise**

218 Using the synthetic spectra, inferred attenuation rates are estimated by least-squares
 219 fitting Eq. 1 with

$$\alpha(f) = -\frac{1}{x_2 - x_1} \ln \left(\frac{E(f, x_2)}{E(f, x_1)} \right) \quad (6)$$

220 at each frequency f using pairs of positions x_1, x_2 . Using $x_1 = 0$ is most consistent with
 221 the definition in Eq. 1, however this is not always measured in field experiments and we
 222 therefore explore the more general case of arbitrary x_1, x_2 with $x_2 > x_1$. There are sev-
 223 eral other options for fitting Eq. 1, though the choice of the fitting method is not impor-
 224 tant for the present study, given that true attenuation rates are known a priori. Inferred
 225 attenuation is then compared with the true attenuation that was specified in producing
 226 the synthetic results, especially in regards to frequency dependence. The overall frequency
 227 dependence b is inferred by least-squares fitting Eq. 2 with

$$b = \frac{\ln f}{\ln(\alpha(f))} \quad (7)$$

228 from the peak frequency f_p of the incident spectrum $E(f, 0)$ to the max frequency ob-
 229 served $f = 0.5$ Hz. This inferred b is somewhat sensitive to the choice of frequency range
 230 for fitting, but it is only meant to show qualitative effects for values relevant to the case
 231 studies. Using frequencies $f > f_p$ centers the results on the tail of the wave energy spec-
 232 trum, where rollovers have been reported in previous studies.

233 **3 Results**

234 The results begin with the general effect of the spurious variance (energy) added
 235 to observed wave energy spectra, followed by the case studies. The energy from noise
 236 causes substantial changes to the shape of the observed attenuation rates, in general, and
 237 for all the cases examined herein. The case studies provide both a practical sense of the
 238 problem, as well as an exploration of the parameter space that cannot be fully described
 239 by the assumptions in the general solution.

240 **3.1 Generalized effects of noise**

241 Combining Eqs. 1 and 3 gives the general form of the observed $\alpha(f)$ as a function
 242 of the true $\alpha_t(f)$ and the ratio of noise energy $E_n(f)$ to the true spectral energy of the
 243 wave signal $E_s(f)$,

$$\alpha(f) = \alpha_t(f) - \frac{1}{x} \ln \left(1 + \frac{E_n(f)}{E_s(f, x)} \right). \quad (8)$$

244 Previous studies have applied a uniform cutoff in $E(f, x)$ (with implied $r = 0$ in Eq. 5)
 245 and discarded any attenuation calculated for $\frac{E_n(f)}{E_s(f, x)} > 1$. The problem is that such a
 246 ratio is unlikely to be constant in frequency. Even for ratios of $\frac{E(f_p)}{E_s(f_p, x)} \sim 1$, the abso-
 247 lute error in $\alpha(f)$ at any particular f may be small, but the error in the dependence on
 248 f may be severe (because the bias grows in f). In particular, if the spectral shapes of
 249 $E_n(f), E_s(f, x)$ diverge, the effects of noise energy will be a strong function of frequency.

Assuming that $E_s(f, x)$ and $E_n(f)$ are both power laws in f , the error in attenuation grows with approximately $\ln(f)$. The specific rate comes from the ratio of the power laws, which is almost assured to be positive given that $E_s(f, x)$ will only steepen from an initial $q = -4$. (There are no known or proposed mechanisms for a natural wave energy spectrum ever to have a slope less than f^{-4} .) The noise spectra have at most a slope of $r = -4$ for accelerometer measurements, and less for other methods. Thus, wave energy in sea ice will tend to decrease with frequency faster than the noise energy decreases with frequency, and a negative bias in attenuation that grows with frequency is almost assured.

The general form of the bias in attenuation is controlled by the ratio

$$\frac{E_n(f)}{E_s(f, x)} \sim f^{r-q}, \quad (9)$$

and thus for any $q < r$ the negative bias in attenuation will grow in frequency. Figure 2 illustrates the attenuation bias for $\frac{H_n}{H_s} = 0.05$ at the peak frequency f_p and various $r - q$ combinations. Given the typical range of $10^{-5} < \alpha(f) < 10^{-3}$, the errors for in Figure 2 are significant. For any attenuation that grows in frequency (Eq. 2), the slope of $E_s(f, x)$ will become more and more negative in ice (i.e., $q < -4$) and thus for any reasonable range of noise shape ($-4 < r < 0$), the ratio will grow. Thus it is only for the rare case of a constant true attenuation that maintains $q = -4$ within the ice and noise shape of $r = -4$ that the bias in observed attenuation will be constant. In some conditions the growing bias may only be sufficient to flatten the observed attenuation rates; in others, it will cause an apparent rollover in attenuation at high frequencies. This flattening is expected for the particular case of an open water $E(f, x = 0)$ that is used for all attenuation calculations, since both exponents q, r will tend to -4 .

Another mechanism by which $E_s(f, x)$ could retain the f^{-4} shape for all x is through wind input, which is often discussed in relation to the spectral shape of wave attenuation in sea ice. If wind input in sea ice was analogous to the equilibrium concepts of Phillips (1985), then $E_s(f, x) \sim f^{-4}$ could be maintained, even as the overall $E_s(f, x)$ was reduced by an attenuation that was not constant in frequency. Even with wind input, f^{-4} remains a bound on the slope of the true wave spectra. Figure 2 shows that even in such conditions, the negative bias in $\alpha(f)$ is likely to grow in frequency, and thus the shape of inferred $\alpha(f)$ will be altered.

The spatial dependence $\frac{1}{x}$ in Eq. 8 is also worth noting, since it may cause severe bias at short distances even when the ratio $\frac{E_n(f)}{E_s(f, x)}$ is small. Indeed, Li et al. (2017) note changes in the rollover period for different distances that may be related to the attenuation bias changing with $\frac{1}{x}$. Figure 2 uses a distance of $x = 10$ km, which is within the range of all field experiments discussed herein.

The role of distance and the effect of true spectra $E_s(f, x)$ that steepen beyond $q = -4$ within ice are explored in the case studies that follow, using the parameters in Table 1. There are figures and descriptions for each case, following a standard format. Each case has some range of x and f for which the noise has a strong effect on the inferred $\alpha(f)$. However, the significant wave heights are rarely affected by the noise, even far within the ice. The practical result is that noise energy remains a small fraction of the total energy for all cases, but it has significant effects on the spectral shape of inferred attenuation. In summary, noise can affect H_s no more than the value of H_n , but noise can make the apparent α go all the way to zero.

3.2 CODA 2019

The Chukchi Sea CODA 2019 case study results are shown in Figure 3. Panel (a) shows true spectra that steepen with distance into the ice, and panel (b) shows observed spectra that begin to approach the $r = -4$ noise floor slope at the highest frequencies.

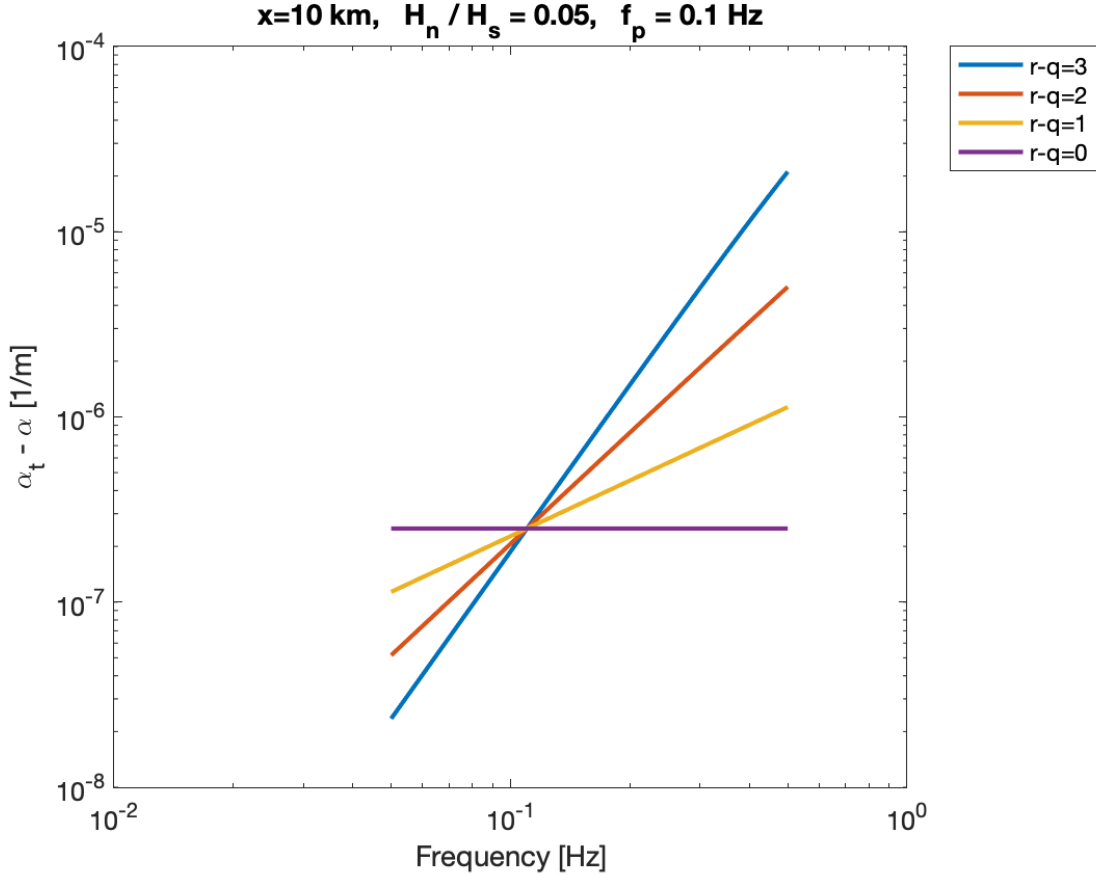


Figure 2. Bias in observed $\alpha(f)$ as a function of frequency for combined signal and noise exponents $r - q$. Example shown is for a distance of 10 km into the sea ice and a ratio of noise to true wave heights $H_n/H_s = 5\%$.

298 In panel (c), the attenuation rates estimated from the observations (Eq. 6) have a neg-
 299 ative bias that flattens the frequency response away from the true attenuation. Thus the
 300 fitted exponent shown in panel (e) deviates from the true $b = 2$ with increasing distance
 301 into the ice. In panel (d), the observed wave heights agree well with the true wave heights.

302 This case study is a best-case scenario, in which the negative bias in attenuation
 303 is small and limited to flattening $\alpha(f)$ at a few frequencies. This is because the noise is
 304 steep ($r = -4$) and the distances are short ($0 < x < 6$ km) such that the true energy
 305 spectra do not become much steeper than f^{-4} .

306 3.3 Sea State 2015

307 The Sea State 2015 case study results are shown in Figure 4. Panel (a) shows true
 308 spectra that steepen dramatically with the longer distances into the ice, and panel (b)
 309 shows observed spectra that clearly tend to the $r = -4$ noise floor slope at many fre-
 310 quencies. In panel (c), the attenuation rates estimated from the observations (Eq. 6) have
 311 a negative bias that flattens the frequency response away from the true attenuation ($b =$
 312 2). This trend is similar to the Cheng et al. (2017) results from analyzing the actual field
 313 data, in which a flattening of $\alpha(f)$ is evident for $f > 0.3$ Hz in their Figure 4. Cheng
 314 et al. (2017) attributed this flattening to wind input; here, we show that it is more likely

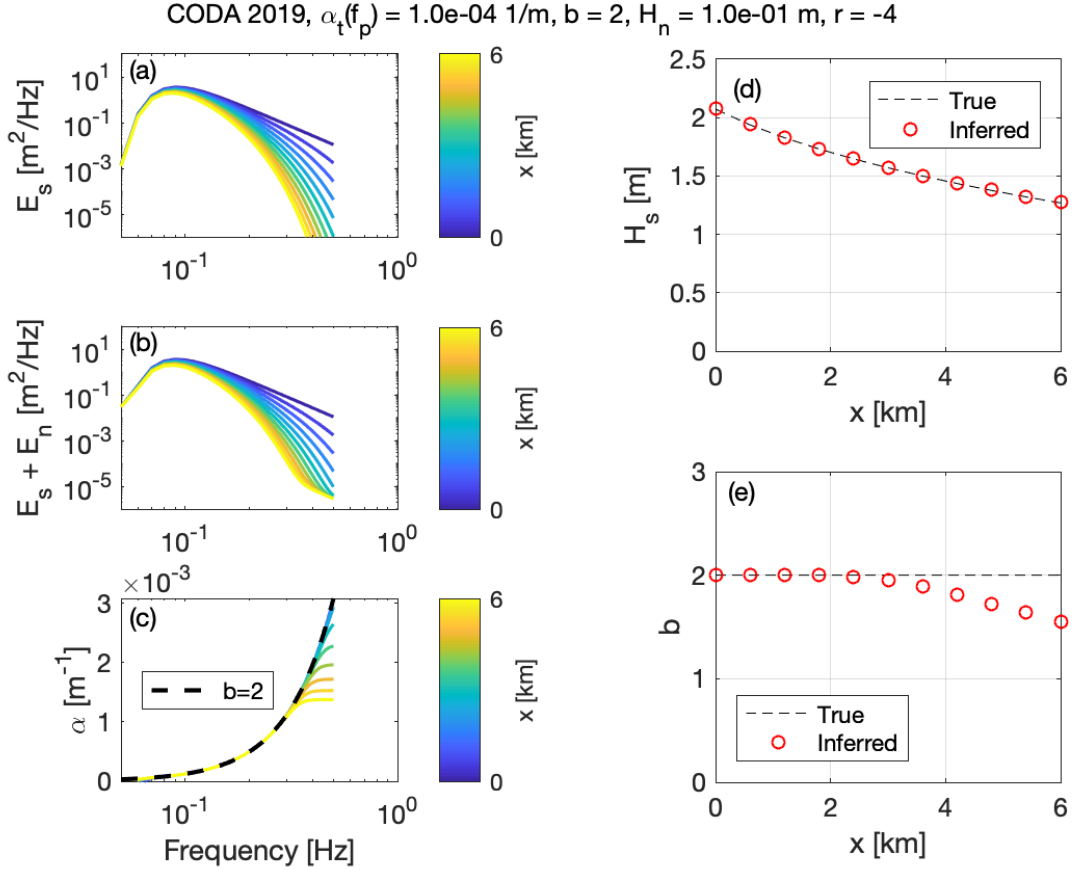


Figure 3. Synthetic results for the Chukchi Sea CODA 2019 case study. (a) true wave energy spectra (colors show distance into the ice). (b) observed wave energy spectra with noise added (colors show distance into ice). (c) true attenuation rate (black dashed line) and observed attenuation rate (colors show distance into ice). (d) wave heights as a function of distance into the ice that are specified as true (black dashed line) and observed (red circles). (e) exponent of frequency power law in attenuation that is determined from observations (red circles) and specified as true (black dashed line).

315 caused by negative bias from spectral noise in the observations. In both the synthetic
 316 observations and the actual field observations, a full rollover in the observed α does not
 317 occur. The $r = -4$ shape of the noise is only sufficient to flatten α in frequency; a full
 318 rollover (decrease of $\alpha(f)$ in frequency) would require noise with a different shape (i.e.,
 319 $r = -2$ or $r = 0$). As the spurious flattening of $\alpha(f)$ expands in frequency, the fitted
 320 exponent b shown in panel (e) deviates from the true $b = 2$ with increasing distance
 321 into the ice. Despite the noticeable bias in $\alpha(f)$, the observed wave heights agree well
 322 with the true wave heights (Figure 4d).

323 3.4 SIPEX 2012

324 The Antarctic MIZ 2012 case study results are shown in Figure 5. All of the observed
 325 spectra in panel (b) are effected by noise energy, even though the imposed noise
 326 height is only $H_n = 3$ cm. In panel (c), the observed attenuation rates have a clear rollover
 327 in frequency that is spurious relative to the $b = 2$ dependence of the true attenuation.

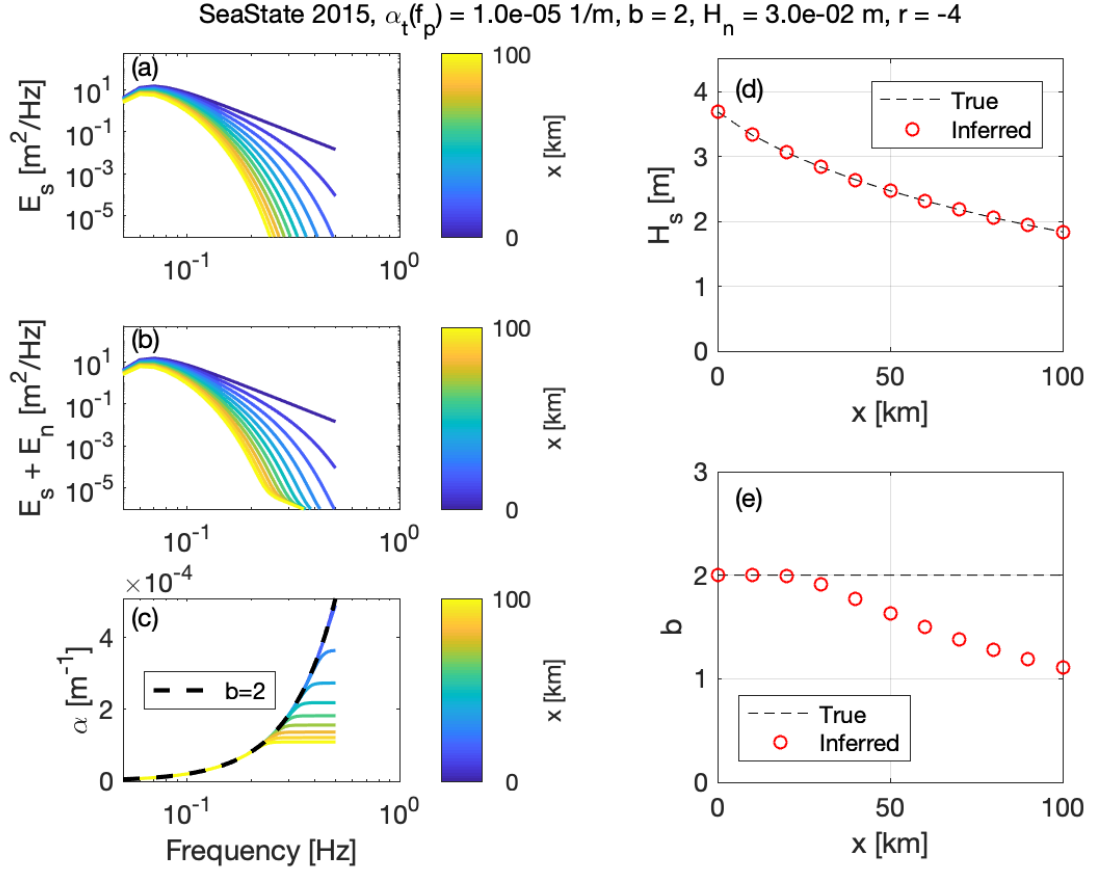


Figure 4. Synthetic results for the Beaufort Sea State 2015 case study. Panels as in Figure 3.

328 Panel (e) shows severe bias in the fitted b because of the spurious rollover. This is sim-
 329 ilar to the rollovers reported in (Li et al., 2017), though that study attributes the rollovers
 330 to wind input. Here, the noise bias causes a spurious rollover that shifts to lower frequen-
 331 cies at longer distances; that pattern is qualitatively consistent with rollover patterns re-
 332 ported in Li et al. (2017). In panel (d), the observed wave heights continue to agree well
 333 with the true wave heights, because H_n is small.

334 We can repeat the approach of Meylan et al. (2014), who analyzed the actual field
 335 observations using a constant cutoff $E(f) > 10^{-2}$ m^2/Hz that is well above the imposed
 336 $E_n(f)$ at any frequency. That applies a constraint $\frac{E_n(f)}{E(f,x)} \ll \frac{1}{10}$ at all frequencies. With
 337 this new constraint, the synthetic observations no longer have much rollover in observed
 338 attenuation rates (not shown). However, the cutoff creates severe limitations on the fre-
 339 quencies f that can be analyzed at any particular distance x . The higher frequencies ($f >$
 340 0.15 Hz) have energies below the cutoff at all x , and thus no attenuation values are cal-
 341 culated for those frequencies.

342 3.5 STiMPI 2000

343 The Weddell Sea STiMPI 2000 case study results are shown in Figure 6. The spec-
 344 ified noise energy clearly affects the observed spectra in panel (b), relative to the true
 345 spectra in panel (a). In panel (c), the noise bias causes spurious rollovers in the observed
 346 attenuation rates which are similar to the rollovers reported in the Li et al. (2017) anal-

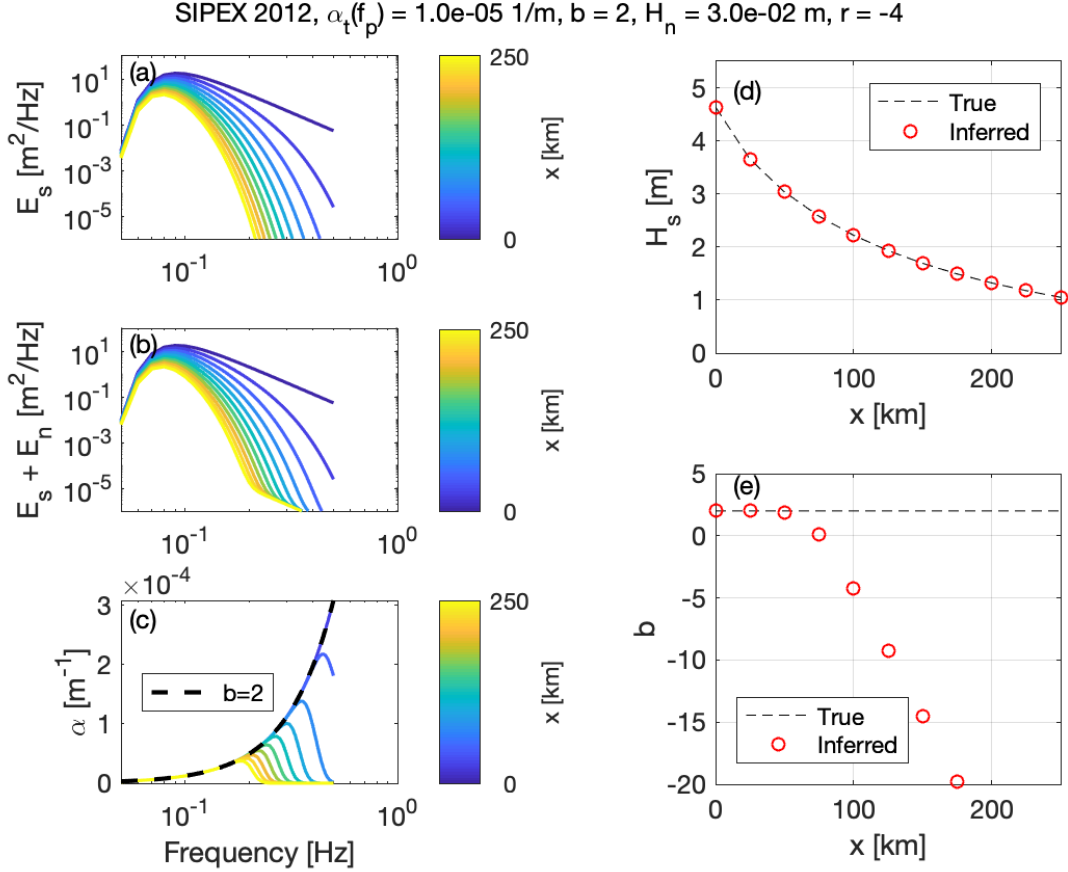


Figure 5. Synthetic results for the Antarctic SIPEX 2012 case study. Panels as in Figure 3.

347 ysis of the actual field data. The fitted exponent shown in panel (e) rapidly deviates from
 348 the true $b = 3$ with increasing distance into the ice, where $b = 3$ is specified instead
 349 of $b = 2$ following the results in Meylan et al. (2018). The noise bias is sufficient to cause
 350 the apparent rollover. For both of these cases addressed in Li et al. (2017), it may be
 351 that noise bias and wind input contribute together in producing apparent rollovers in
 352 attenuation rates. Again, in panel (d), the observed wave heights agree well with the true
 353 wave heights.

354 4 Discussion

355 Results suggest that negative bias in attenuation rates at high frequencies is a com-
 356 mon issue for most field observations. Along with wind input and nonlinear mechanisms
 357 that may affect the high-frequency tail of ocean wave spectra, spurious energy from in-
 358 strument noise is an explanation for all of the rollovers in attenuation that have been
 359 reported in the literature.

360 The following guidelines are recommended for future use of field observations in
 361 the estimation of spectral attenuation rates:

- 362 • Do not apply a constant cutoff in spectral wave energy, as this implies a flat noise
 363 spectrum ($r = 0$) that is unlikely for most observations.

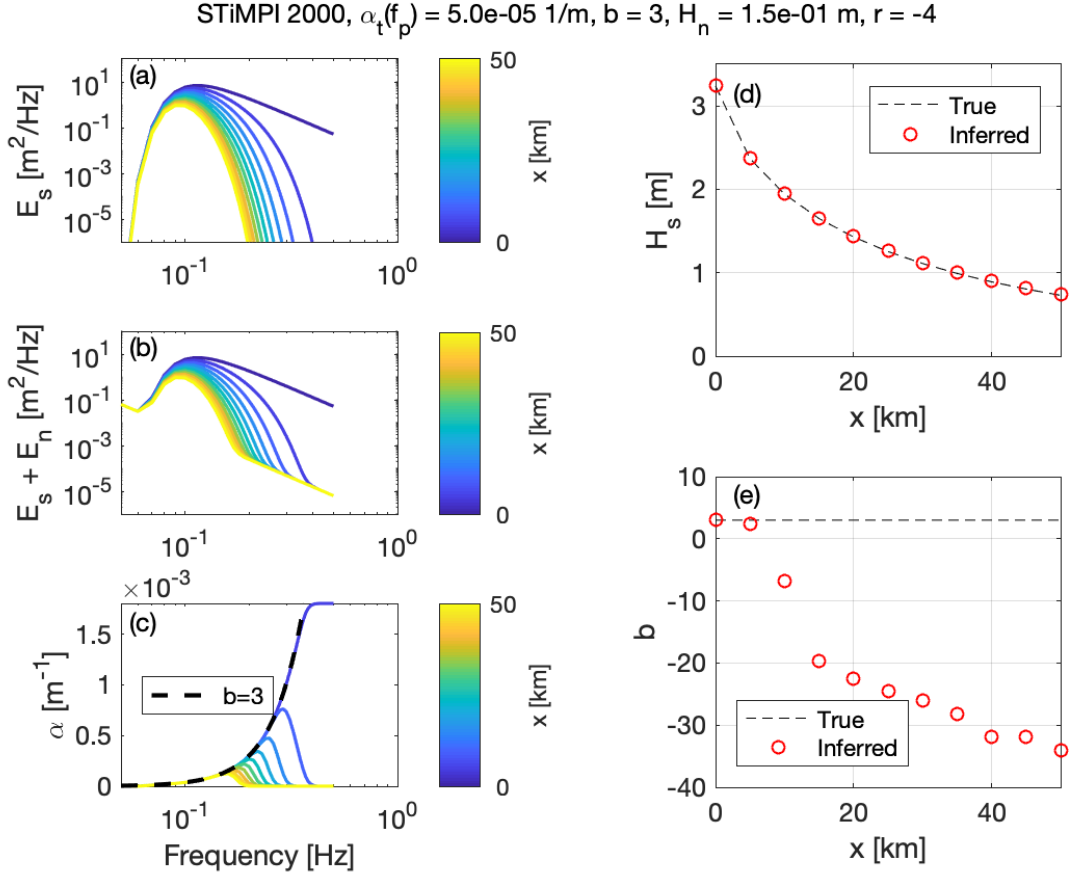


Figure 6. Synthetic results for the Weddell Sea STIMPI 2000 case study. Panels as in Figure 3.

- 364
- 365
- 366
- 367
- 368
- 369
- Determine the spectral shape of the noise empirically, including any filters used in post-processing and the deployment specifics.
 - Consider the ratio $E_n(f)/E_s(f, x)$ as a function of frequency and location, and avoid calculations of attenuation for *any* observation with appreciable $\frac{E_n(f)}{E(f, x)}$.
 - Check for convergence of attenuation results applying minimum $E(f)$ cutoffs as $\frac{E_n(f)}{E(f, x)} \rightarrow 0$.

370 The deployment specifics in the second point are particularly important, given the com-
 371 mon practice of placing wave measurement devices on ice floes. The hydrodynamic re-
 372 sponse of ice floes will depend on their dimensions and mass, such that they may have
 373 a damped response at high frequencies and the noise floor may be elevated relative to
 374 testing a device floating in open water. The frequencies affected can be estimated fol-
 375 lowing the methods of Thomson et al. (2015), who report on the analogous condition of
 376 a wave buoy with a dramatic increase in size resulting from biofouling.

377 It is important to restate that the noise bias reported herein has a negligible ef-
 378 fect on the total energy (and thus wave heights). Bulk attenuation rates can be deter-
 379 mined robustly, even in the presence of noise. It is the spectral tail (high frequencies)
 380 in which much care is required.

381 4.1 Noise effects at low frequencies

382 Although the focus herein is on high frequencies, energy from noise also can bias
 383 attenuation results at low frequencies. As shown in Figure 1, the f^{-4} shape appears to
 384 persist at low frequencies, though the actual level may vary depending on filters applied
 385 to reduce drift in the raw accelerometer data. We thus include a brief investigation of
 386 low-frequency noise bias by recalculating the attenuation coefficients from SIPEX 2012,
 387 as published in Meylan et al. (2014).

388 We note that the original data analysis in Meylan et al. (2014) was based on a fre-
 389 quency independent noise cut off ($r = 0$). In that analysis the noise floor was set suf-
 390 ficiently high to avoid the roll over; indeed no analysis was completed for any periods
 391 $T < 6$ s (or $f > 0.15$ Hz). Although sufficiently conservative to avoid spurious calcu-
 392 lations in the high-frequency tail, this cutoff had a secondary effect of suppressing mea-
 393 surements which were valid for long periods. Figure 7 shows the sensitivity to the noise
 394 cutoff by comparing the median attenuation with a fixed noise floor cutoff ($r = 0$, as
 395 used in Meylan et al. (2014)) and using three different levels of noise floor cutoffs that
 396 are empirical power laws in frequency ($r = -4$).

397 The left panels of Figure 7 show attenuation results with three different levels of
 398 f^{-4} cutoff applied. The right panels show the median attenuation as a function of pe-
 399 riod for the two of the three levels. The black curves are from the original analysis of
 400 Meylan et al. (2014), for comparison. The constant noise floor applied in original anal-
 401 ysis lowered the attenuation at short periods and raised it at long periods. The correct
 402 analysis is the lower right panel, and the blue line is the fit to the power law. This anal-
 403 ysis suggests a power law with $b = 3$ for the true attenuation, which is within the range
 404 of expected exponents (Meylan et al., 2018).

405 Just as the negative bias in attenuation rate at high frequencies results from ex-
 406 ponents $r - q > 0$, the positive bias in attenuation rate at low frequencies is the con-
 407 sequence of $r - q < 0$. At these low frequencies, the noise energy $E_n(f)$ is more steep
 408 than the signal energy $E_s(f)$, because the signal is outside of the equilibrium wind wave
 409 range. The general result is the same: the frequency dependence of the attenuation rates
 410 will be sensitive to the noise cutoff, even when the absolute error in the attenuation rates
 411 is small.

412 5 Conclusions

413 Instrument noise in wave measurements causes a bias in attenuation rates that man-
 414 ifests in spurious relations between frequency and attenuation rates. This is sufficient
 415 to explain the rollover in attenuation rates observed for several studies from a variety
 416 of different wave-ice buoys. A general form of the noise bias (Eq. 8) can be applied to
 417 avoid this issue in future analysis.

418 Acknowledgments

419 Funded by the National Science Foundation (OPP-1818485) as part of the Coastal Ocean
 420 Dynamics in the Arctic project. Erick Rogers provided valuable feedback and discussions
 421 during the preparation of the manuscript. The CODA project is detailed at <http://www.apl.uw.edu/coda>,
 422 and the CODA 2019 data will be available at the Arctic Data Center. The Arctic Sea
 423 State project is detailed at <http://www.apl.uw.edu/arcticseastate>, and the 2015 data are
 424 available at <https://digital.lib.washington.edu/researchworks/handle/1773/41864>. SIPEX
 425 data are available at <http://dx.doi.org/doi:10.4225/15/53266BEC9607F>. STiMPI were
 426 provided by Martin Doble (Polar Scientific, Ltd.).

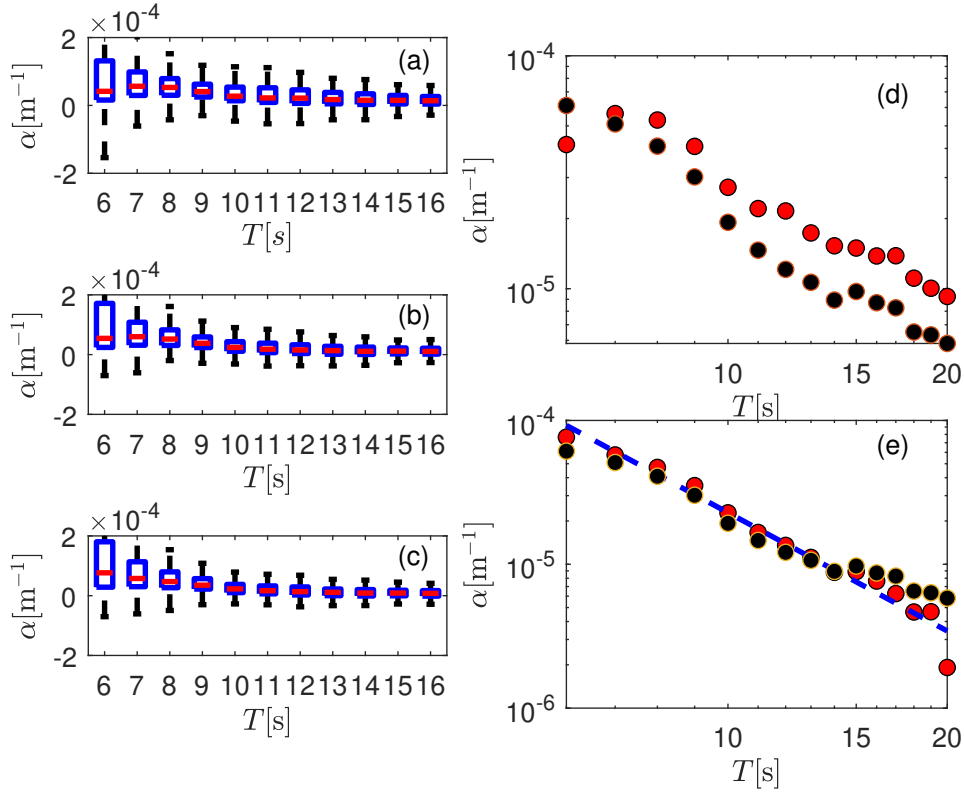


Figure 7. Low-frequency attenuation rates from SIPEX as a function of wave period applying noise cutoffs of (a) $E(f)f^{-4} < 10^{-8}$, (b) $E(f)f^{-4} < 10^{-7}$, and (c) $E(f)f^{-4} < 10^{-6}$. (d) The median attenuation rates (red dots) for $E(f)f^{-4} < 10^{-8}$ and the results from the previous analysis in (Meylan et al., 2014) (black dots). (e) The median attenuation rates (red dots) for $E(f)f^{-4} < 10^{-6}$ (which is the correct noise floor shown in Figure 1) and the results from the previous analysis in (Meylan et al., 2014) (black dots). The blue dotted line is the straight line fit to the red dots, $\alpha(f) \sim f^3$.

References

427

- 428 Alves, J. H. G. M., Banner, M. L., & Young, I. R. (2003, 2014/02/01). Revisiting
 429 the Pierson–Moskowitz asymptotic limits for fully developed wind waves. *J.*
 430 *Phys. Oceanogr.*, *33*(7), 1301–1323. doi: 10.1175/1520-0485(2003)033<1301:
 431 RTPALF>2.0.CO;2
- 432 Ardhuin, F., Otero, M., Merrifield, S., Grouazel, A., & Terrill, E. (2020). Ice break-
 433 up controls dissipation of wind-waves across southern ocean sea ice. *Geophys-*
 434 *ical Research Letters*, n/a(n/a), e2020GL087699. Retrieved from [https://](https://agupubs.onlinelibrary.wiley.com/doi/abs/10.1029/2020GL087699)
 435 agupubs.onlinelibrary.wiley.com/doi/abs/10.1029/2020GL087699
 436 (e2020GL087699 2020GL087699) doi: 10.1029/2020GL087699
- 437 Cheng, S., Rogers, W. E., Thomson, J., Smith, M., Doble, M. J., Wadhams, P.,
 438 ... Shen, H. H. (2017). Calibrating a viscoelastic sea ice model for wave
 439 propagation in the arctic fall marginal ice zone. *Journal of Geophysical Re-*
 440 *search: Oceans*, *122*, n/a–n/a. Retrieved from [http://dx.doi.org/10.1002/](http://dx.doi.org/10.1002/2017JC013275)
 441 [2017JC013275](http://dx.doi.org/10.1002/2017JC013275) doi: 10.1002/2017JC013275
- 442 Doble, M. J., De Carolis, G., Meylan, M. H., Bidlot, J.-R., & Wadhams, P. (2015).
 443 Relating wave attenuation to pancake ice thickness, using field measurements
 444 and model results. *Geophysical Research Letters*, *42*(11), 4473–4481. Retrieved
 445 from <http://dx.doi.org/10.1002/2015GL063628> (2015GL063628) doi:
 446 [10.1002/2015GL063628](http://dx.doi.org/10.1002/2015GL063628)
- 447 Herbers, T. H. C., Jessen, P. F., Janssen, T. T., Colbert, D. B., & MacMahan, J. H.
 448 (2012). Observing ocean surface waves with GPS tracked buoys. *J. Atmos.*
 449 *Ocean. Tech.*, *29*. doi: 10.1175/JTECH-D-11-00128.1
- 450 Kohout, A. L., Penrose, B., Penrose, S., & Williams, M. J. (2015). A device for meas-
 451 uring wave-induced motion of ice floes in the antarctic marginal ice zone. *An-*
 452 *nals of Glaciology*, *56*(69), 415–424. doi: 10.3189/2015AoG69A600
- 453 Kohout, A. L., Williams, M. J. M., Dean, S. M., & Meylan, M. H. (2014, 05 28).
 454 Storm-induced sea-ice breakup and the implications for ice extent. *Nature*,
 455 *509*, 604 EP -. Retrieved from <http://dx.doi.org/10.1038/nature13262>
- 456 Lenain, L., & Melville, W. K. (2017). Measurements of the directional spectrum
 457 across the equilibrium saturation ranges of wind-generated surface waves.
 458 *Journal of Physical Oceanography*, *47*(8), 2123–2138. Retrieved from [https://](https://doi.org/10.1175/JPO-D-17-0017.1)
 459 doi.org/10.1175/JPO-D-17-0017.1 doi: 10.1175/JPO-D-17-0017.1
- 460 Li, J., Kohout, A. L., Doble, M. J., Wadhams, P., Guan, C., & Shen, H. H. (2017).
 461 Rollover of apparent wave attenuation in ice covered seas. *Journal of Geophys-*
 462 *ical Research: Oceans*, n/a–n/a. Retrieved from [http://dx.doi.org/10.1002/](http://dx.doi.org/10.1002/2017JC012978)
 463 [2017JC012978](http://dx.doi.org/10.1002/2017JC012978) doi: 10.1002/2017JC012978
- 464 Masson, D., & LeBlond, P. (1989). Spectral evolution of wind-generated surface
 465 gravity waves in a dispersed ice field. *J. Fluid Mech.*, *202*(111), 43–81.
- 466 Meylan, M. H., Bennetts, L. G., & Kohout, A. L. (2014). In situ measurements
 467 and analysis of ocean waves in the antarctic marginal ice zone. *Geophysical*
 468 *Research Letters*, n/a–n/a. Retrieved from [http://dx.doi.org/10.1002/](http://dx.doi.org/10.1002/2014GL060809)
 469 [2014GL060809](http://dx.doi.org/10.1002/2014GL060809) doi: 10.1002/2014GL060809
- 470 Meylan, M. H., Bennetts, L. G., Mosig, J. E. M., Rogers, W. E., Doble, M. J., & Pe-
 471 ter, M. A. (2018). Dispersion relations, power laws, and energy loss for waves
 472 in the marginal ice zone. *Journal of Geophysical Research: Oceans*, *123*(5),
 473 3322–3335. Retrieved from [https://agupubs.onlinelibrary.wiley.com/](https://agupubs.onlinelibrary.wiley.com/doi/abs/10.1002/2018JC013776)
 474 [doi/abs/10.1002/2018JC013776](https://agupubs.onlinelibrary.wiley.com/doi/abs/10.1002/2018JC013776) doi: 10.1002/2018JC013776
- 475 Phillips, O. M. (1985). Spectral and statistical properties of the equilibrium range in
 476 wind-generated gravity waves. *J. Fluid Mech.*, *156*, 495–531.
- 477 Polnikov, V. G., & Lavrenov, I. V. (2007, Jun 01). Calculation of the nonlinear
 478 energy transfer through the wave spectrum at the sea surface covered with
 479 broken ice. *Oceanology*, *47*(3), 334–343. Retrieved from [https://doi.org/](https://doi.org/10.1134/S0001437007030058)
 480 [10.1134/S0001437007030058](https://doi.org/10.1134/S0001437007030058) doi: 10.1134/S0001437007030058
- 481 Rogers, W. E., Thomson, J., Shen, H. H., Doble, M. J., Wadhams, P., & Cheng,

- 482 S. (2016). Dissipation of wind waves by pancake and frazil ice in the au-
 483 tumn beaufort sea. *Journal of Geophysical Research: Oceans*, 121(11), 7991–
 484 8007. Retrieved from <http://dx.doi.org/10.1002/2016JC012251> doi:
 485 10.1002/2016JC012251
- 486 Squire, V. A. (2007). Of ocean waves and sea ice revisited. *Cold Regions Sci. Tech.*,
 487 49, 110-133.
- 488 Squire, V. A. (2020). Ocean wave interactions with sea ice: A reappraisal. *Annual*
 489 *Review of Fluid Mechanics*, 52(1), null. Retrieved from [https://doi.org/](https://doi.org/10.1146/annurev-fluid-010719-060301)
 490 [10.1146/annurev-fluid-010719-060301](https://doi.org/10.1146/annurev-fluid-010719-060301) doi: 10.1146/annurev-fluid-010719-
 491 -060301
- 492 Thomson, J. (2012, 2013/01/03). Wave breaking dissipation observed with SWIFT
 493 drifters. *Journal of Atmospheric and Oceanic Technology*, 29(12), 1866–1882.
 494 doi: 10.1175/JTECH-D-12-00018.1
- 495 Thomson, J., Ackley, S., Girard-Ardhuin, F., Ardhuin, F., Babanin, A., Boutin, G.,
 496 ... Wadhams, P. (2018). Overview of the arctic sea state and boundary layer
 497 physics program. *Journal of Geophysical Research: Oceans*, 123(12), 8674-
 498 8687. Retrieved from [https://agupubs.onlinelibrary.wiley.com/doi/abs/](https://agupubs.onlinelibrary.wiley.com/doi/abs/10.1002/2018JC013766)
 499 [10.1002/2018JC013766](https://agupubs.onlinelibrary.wiley.com/doi/abs/10.1002/2018JC013766) doi: 10.1002/2018JC013766
- 500 Thomson, J., D'Asaro, E. A., Cronin, M., Rogers, E., Harcourt, R., & Scherbina,
 501 A. (2013). Waves and the equilibrium range at Ocean Weather Station P. *J.*
 502 *Geophys. Res.*, 118, 1-12.
- 503 Thomson, J., Talbert, J., de Klerk, A., Brown, A., Schwendeman, M., Goldsmith,
 504 J., ... Meinig, C. (2015, 2015/06/18). Biofouling effects on the response of a
 505 wave measurement buoy in deep water. *Journal of Atmospheric and Oceanic*
 506 *Technology*, 32(6), 1281–1286. Retrieved from [http://dx.doi.org/10.1175/](http://dx.doi.org/10.1175/JTECH-D-15-0029.1)
 507 [JTECH-D-15-0029.1](http://dx.doi.org/10.1175/JTECH-D-15-0029.1) doi: 10.1175/JTECH-D-15-0029.1
- 508 Vincent, C. L., Thomson, J., Graber, H. C., & Collins, C. O. (2019). Impact of swell
 509 on the wind-sea and resulting modulation of stress. *Progress in Oceanog-*
 510 *raphy*, 178, 102164. Retrieved from [http://www.sciencedirect.com/](http://www.sciencedirect.com/science/article/pii/S0079661118302209)
 511 [science/article/pii/S0079661118302209](http://www.sciencedirect.com/science/article/pii/S0079661118302209) doi: [https://doi.org/10.1016/](https://doi.org/10.1016/j.pocean.2019.102164)
 512 [j.pocean.2019.102164](https://doi.org/10.1016/j.pocean.2019.102164)
- 513 Wadhams, P. (1975). Airborne laser profiling of swell in an open ice field. *Jour-*
 514 *nal of Geophysical Research (1896-1977)*, 80(33), 4520-4528. Retrieved
 515 from [https://agupubs.onlinelibrary.wiley.com/doi/abs/10.1029/](https://agupubs.onlinelibrary.wiley.com/doi/abs/10.1029/JC080i033p04520)
 516 [JC080i033p04520](https://agupubs.onlinelibrary.wiley.com/doi/abs/10.1029/JC080i033p04520) doi: 10.1029/JC080i033p04520
- 517 Wadhams, P., Squire, V. A., Goodman, D. J., Cowan, A. M., & Moore, S. C. (1988).
 518 The attenuation rates of ocean waves in the marginal ice zone. *J. Geophys.*
 519 *Res*, 93(C6), 6799-6818.